



4–7 July 2016
BINP SB RAS

XAFS spectroscopy - a useful tool for determining structure parameters and the electronic state of various nanosystems

S. Erenburg^{1,2}, S. Trubina¹, E. Kovalenko¹, O. Gerasko¹, K. Zhuravlev^{3,4}, T. Malin³, V Zinovyev³, A. Dvurechenskii^{3,4}, P. Kuchinskaya³, V. Zaikovskii^{4,5}, K. Kvashnina⁶

¹Nikolaev Institute of Inorganic Chemistry SB RAS, Novosibirsk

²Budker Institute of Nuclear Physics, SB RAS, Novosibirsk

³Rzhanov Institute of Semiconductor Physics, SB RAS, Novosibirsk

⁴Novosibirsk State University, Novosibirsk

⁵Boreskov Institute of Catalysis SB RAS, Novosibirsk

⁶European Synchrotron Radiation Facilities, Grenoble, France

The advantage of XAFS

Local structural information around the element of interest can be obtained even from disordered samples, such as nanopowders and solutions.

Superfine dispersity metal

Inclusion compounds, nanopowders

Catalysts, functional materials

Semiconductor nanostructures

Quantum dots, wires, wells, quantum molecules

Functional units in computing, information processing

Nanostructures in Solutions

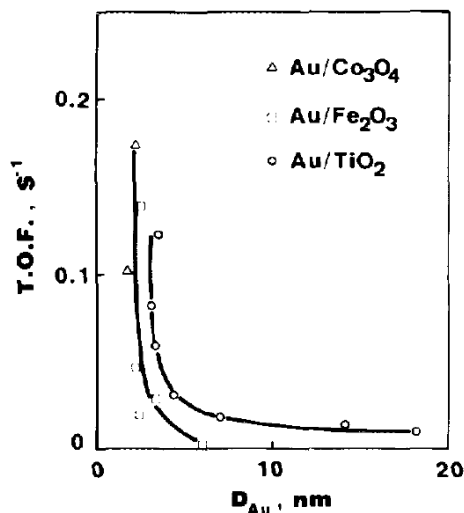
Colloidal particles

Biochemistry, pharmacology

Looking back, we were surprised to find that very promising and advanced new materials and objects, "nano-objects and nanomaterials," have been the subject of research for a long time already.

The research methods that apply synchrotron radiation include our own X-ray absorption spectroscopy were used. EXAFS spectroscopy method that does not require structural periodicity of the order provides special opportunities for studying the structure of nano-systems, which do not have long-range ordering or have limited long-range order.

Structure and catalytic activity of high dispersity metals



Catalytic activity in CO oxidation at 0°C based on surface gold atoms as a function of the mean gold particle diameters.

M. Haruta et al. Low-Temperature Oxidation of CO over Gold Supported on TiO₂, α-Fe₂O₃, and Co₃O₄. J. Catal., 144 (1993) 175.

1974 S.B. Erenburg, A.V. Golovin, S.P. Noskova et al. X-ray absorption K-spectra of high dispersity nickel. *Reactl. Kin. Catal. Lett.* 1, 507.

1978 G.N. Kulipanov, I.A. Ovsyannikova, S.B. Erenburg et al. Issledovanie tonkoy struktury glavnogo kraya pogloshcheniya na SR. (in russian). *Apparatura and metody rent. analiza.* 1, 507.

2007 S.B. Erenburg, B.L. Moroz, N.V. Bausk, V.I. Bukhtiyarov and S. Nikitenko. XAS study on microstructure of Au nanoparticles deposited onto alumina. *Nuclear Instrum. Meth. Phys. Res. A*, 575, 105-108.

S.B. Erenburg, N.V. Bausk, V.V. Bakovets, I.P. Dolgovesova, V.A. Nadolinny and S. Nikitenko. Copper localization in cucurbit[8]uril. *Nuclear Instrum. Meth. Phys. Res., A*, 575, 88-90.

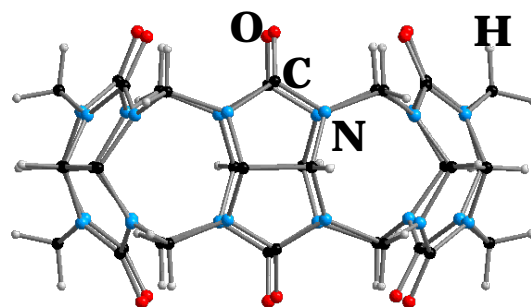
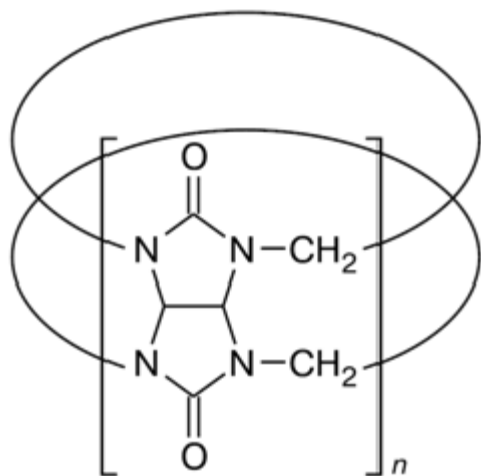
2009 S. Erenburg, S. Trubina, N. Bausk, B. Moroz, A. Kalinkin, V. Bukhtiyarov, S. Nikitenko. Structure of catalytically active gold nanoparticles by XAFS spectroscopy. *Journal of Physics: Conference Series*, 190, 012121.

2013 S.B. Erenburg, S.V. Trubina, E.A. Kovalenko, O.A. Geras'ko, V.I. Zaikovskii, K. Kvashnina, and S.G. Nikitenko. Features of the Microstructure of Gold Nanoparticles inside Cavities of Cucurbit[7]uril According to XAFS Spectra. *JETP Letters*, 97, 5, pp. 285–289.

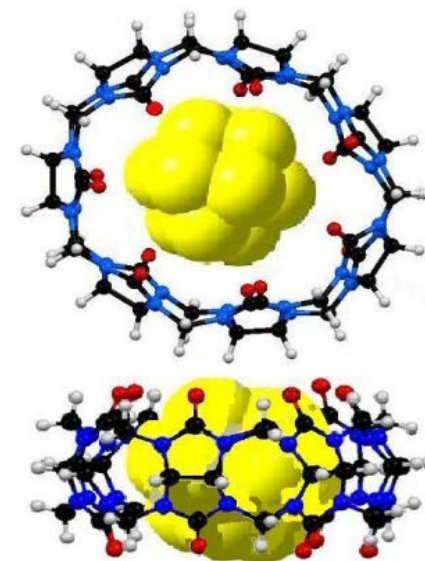
2015 S.B. Erenburg, S.V. Trubina, E.A. Kovalenko, O.A. Geras'ko, V.I. Zaikovskii, D.K. Toporkov, K.O. Kvashnina, and S. G. Nikitenko. Structure and Dimensions of Gold Clusters in Cucurbit[n]uril (CB[n], n=6, 7) Cavities. *J. Surf. Investigation* 10, 45-52.

The last steps of study are in interval from 2013 to 2016 years for systems with cucurbit[n]uril molecules.

Schema of cucurbit[n]uril molecules, $(C_6H_6N_4O_2)_n$, CB[n]



CB[6], $C_{36}H_{36}N_{24}O_{12}$



CB[n], n – number of chain links

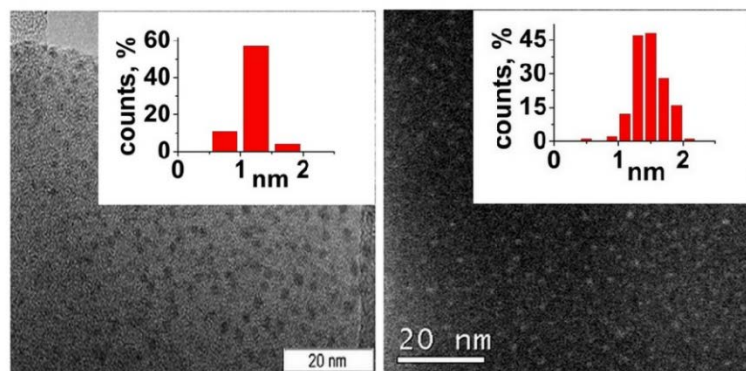
		CB[6]	CB[7]	CB[8]
Cavity diameter - b, Å		5.8	7.3	8.8
Entrance diameter - c, Å		3.9	5.4	6.9
Height - d, Å		9.1	9.1	9.1
Cavity volume - v, Å ³		164	280	480

Lee J.W., Samal S., Selvapalam N. et al. Acc. Chem. Res. 2003, 36 (8), 621.

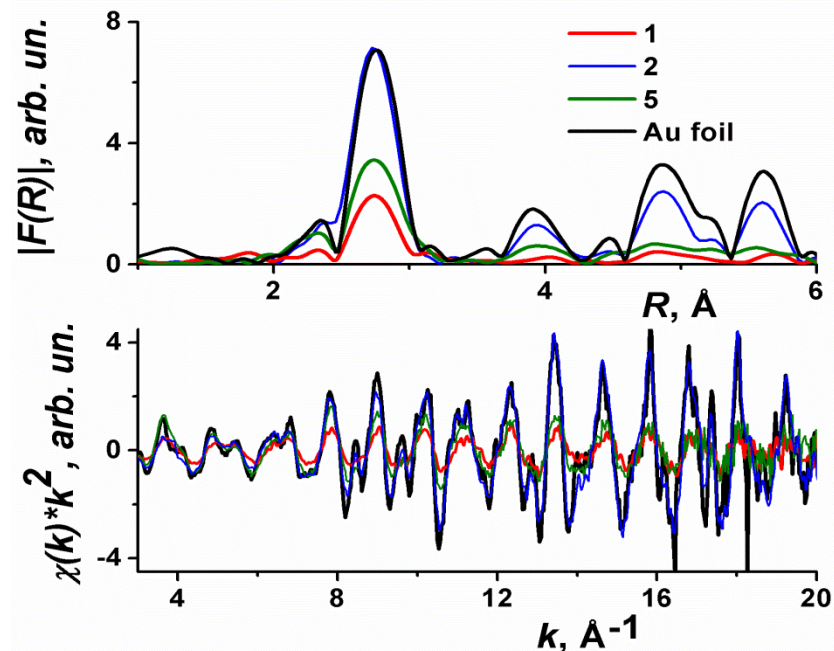
W.A. Freeman et al, J. Am. Chem. Soc. 1981, 103, 7367.

Preparation of Au@CB[6,7]

Gold nanoparticles were encapsulated by using liquid-phase process that involved solutions of CB[7]s in water/ethanol mixture with various $\text{HAuCl}_4 + \text{CB}[7]$ concentration in solution (10^{-3} and 10^{-4} mol/L) and the reduction of HAuCl_4 by NaBH_4 . For dissolution CB[6] in water and obtaining the Au@CB[6]- inclusion compound was used MgCl_2 . After reduction the solution became immediately colored, which indicated the of Au^{III} to form gold nanoparticles. (A. Corma, H. Garc'ia, P. Montes-Navajas et al., Eur. J. B **13**, 6359 (2007)).



TEM photo and bar chart of the Au nanoparticle size distribution for samples 1 (left) and 3 (right).



Experimental $k^2\chi(k)$ AuL_{III} EXAFS spectra of Au@CB[7] samples and Au foil (bottom) and their Fourier transform magnitudes $|FT|$ (hight).

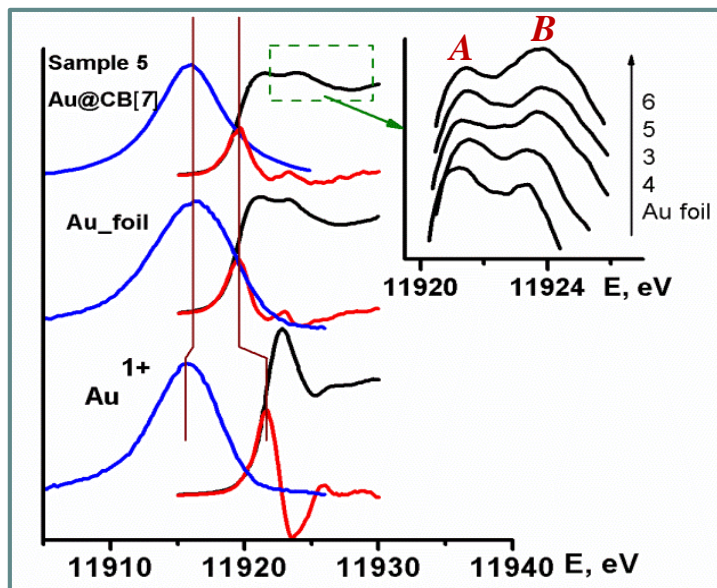
Samples	Initial compounds				
	HAuCl_4 , CB[7], mol/L	Water/ ethanol	NaBH_4 , mol/L	KBH_4 , mol/L	MgCl_2
1	CB[7]	10^{-4}	1:1	0.1	
2	CB[7]	10^{-3}	1:1	0.1	
3	CB[7]	10^{-4}	1:1	0.1	
4	CB[6]	10^{-4}	1:0	0.1	+
5	CB[7]	10^{-4}	1:1		0.1
6	CB[7]	10^{-4}	1:1		0.1

Electron and spatial structure Au@CB[6,7]

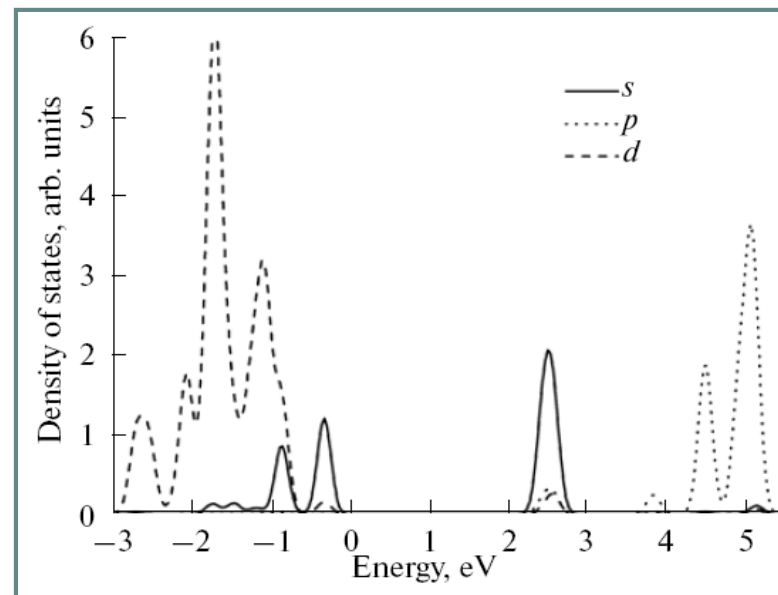
Sample	N_1	N_2	$R_1, \text{Å}$	$R_2, \text{Å}$	$2\sigma^2, \text{Å}^2, 297 \text{ K}$	$2\sigma^2, \text{Å}^2, 12 \text{ K}$	$L_3 \text{ edge}$
1 CB[7]	12 (15%)	6.1 (85%)	2.87	2.84	0.023	0.0073	11919.57
2 CB[7]	11.9	-	2.87	-	0.017	0.0045	11919.56
3 CB[7]	12 (65%)	5.7 (35%)	2.87	2.84	0.018		11919.58
4 CB[6]	12 (89%)	5.1 (11%)	2.87	2.84	0.020		11919.58
5 CB[7]	12 (55%)	8.7 (45%)	2.87	2.85		0.0086	11919.58
6 CB[7]	12 (70%)	7.8 (30%)	2.87	2.85		0.0090	11919.50
Au_foil	12		2.872		0.016	0.0030	11919.56
Au ¹⁺							11921.69

$N_{1,2}$ - the coordination numbers, $R_{1,2}$ - Au-Au interatomic distances, σ^2 - the Debye-Waller factor. Red color figures correspond to the fixed values of N_I and R_I . $\Delta R = 1.5 - 3.2 \text{ Å}$; $S_0^2 = 0.82$

As is shown by the visual HRTEM control, **in all samples studied, apart from a significant contribution of finely dispersed particles with sizes of ~1 nm, presents some amount of larger gold particles with sizes of ~5 - 10 nm.** Microstructural parameters for this particles was detected close to the bulk metal parameters. As seen from the Table, small gold clusters in the CB[6, 7] cavities are characterized by slightly shorter (**by 0.03 Å**) interatomic distances and considerably larger Debye–Waller factors as compared to bulk Au. The average coordination numbers for Au atoms in the clusters of Au@CB[7] inclusion compounds are $N_{\text{small}} \sim 6$ ($D \sim 8 \text{ Å}$) and $N_{\text{small}} \sim 5$ ($D \sim 7 \text{ Å}$) **for Au@CB[6]**. The structural parameters for sample 2 with the average Au cluster size $D_{\text{av}} \sim 10 \text{ nm}$ are close to the parameters of bulk gold foil. **No visible ($\pm 0.02 \text{ eV}$) shifts of the Au L_{III} absorption edges were detected for the samples with Au@CB[6, 7] containing gold nanoclusters in comparison with gold foil.**

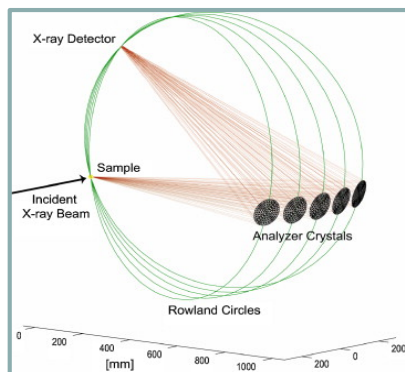


On the left: Au L_{III} HERFD spectra – black lines, first derivatives of Au L_{III} HERFD spectra – red lines, spectra of the valence band (Au $L_{\beta 5}$, 5d – 2p transition)– blue lines. **On the right:** maxima of the Au L_{III} HERFD “white line” of samples Au@CB[6, 7] and Au foil (absorption coefficients).



Theoretical densities of atomic states and “band gap” for the Au₃₂ cluster. (B3LYP/LANL2DZ approximation, GAUSSIAN software).

In a number of theoretical (Yarzhemsky, V.G.; Murav’ev, E.N.; Kazaryan, M.A. et al. 2012 *Inorg. Mater.* 48, 1075) and experimental (Li, J.; Li, X.; Zhai, H.-J.; Wang, L.-S. 2003 *Science*. 299, 864) works a band gap of ~1.5– 2.0 eV was found between the occupied and unoccupied states for gold nanoclusters. **The detected changes in the structure of unoccupied electronic states of the samples containing small gold clusters (a noticeable increase in the intensity of the B peak) seem to be due to the size effect and the appearance of the ~1.5– 2.0 eV band gap.** This gap can be the reason for the special physical (optical) and chemical (catalytic) properties of small gold clusters.

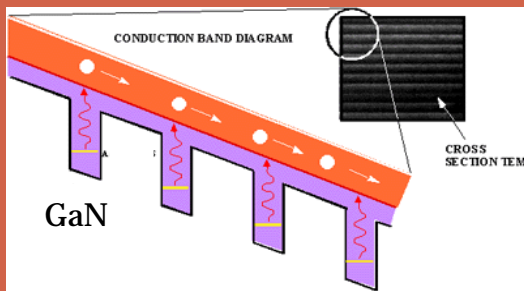
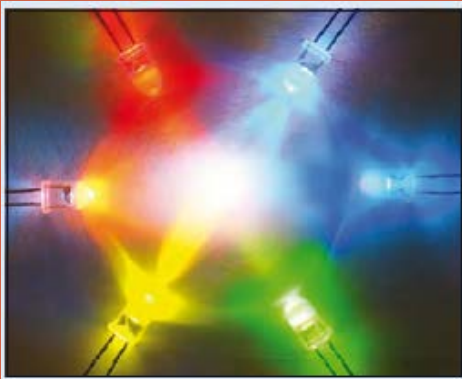


The scheme of second (X-ray emission) spectrometer with vertical scattering geometry. The focusing (Rowland) circles are shown. Only one channel of relaxation (Au La) of X-ray excited state is used, **that increases its lifetime and decreases the width of the level (uncertainty relation).**

Discussion and conclusion about Au@CB[6, 7]

- No visible (± 0.02 eV) shifts of the AuL_{III} absorption edges, changes in the AuL_{III} white line intensity, and hence changes in the charge state of gold were detected for the samples with Au@CB[6, 7] containing gold nanoclusters in comparison with gold foil and the samples containing large particles.
- It is found that gold clusters in the CB[6, 7] cavities are characterized by appreciably smaller (by $\sim 0.03 \text{ \AA}$) interatomic distances and considerably larger (three times and more at 12 K) Debye-Waller factors as compared to bulk Au. Hence for small gold particles structural stresses and structure disordering become substantial. These structural changes are likely to be the reason for the appearance of the catalytic activity of gold during its dispersion to the sizes $D < 3\text{-}5$ nm.
- It is found that the reason for the special physical (optical) and chemical (catalytic) properties of small gold clusters can be the properties related to the size effect with the appearance of the band gap between the occupied and unoccupied electronic states.

GaN/AlN multiple quantum wells



GaN/AlN multiple quantum wells (MQW) are promising materials for novel optical applications:

- ultraviolet emitting and detector devices;
- intersubband devices for infrared applications.

1984 Л.Н.Мазалов, А.Я.Рояк, С.Б. Эренбург и др. Применение рентгеновской спектроскопии для изучения особенностей электронного строения поверхности и приповерхностных слоев. Рост полупроводниковых кристаллов и пленок, ч.I. Новосибирск, Наука, с. 104-131.

2001 S.B.Erenburg, N.V.Bausk, N.P.Stepina, et al. Microscopic parameters of heterostructures containing nanoclusters and thin layers of Ge in Si matrix, Nucl. Instr. & Meth. Phys. Res. A., 470/1-2, 283.

2003 S. Erenburg, N. Bausk, L. Mazalov et al. Ge quantum dots structural peculiarities depending on the preparation conditions. J. Synchrotron Rad., 10, 380.

2005 S.B. Erenburg, N.V. Bausk, L.N. Mazalov et al. Quantum dots microstructure and energy spectrum peculiarities. Physica Scripta, 115, 439.

2007 S.B. Erenburg, N.V. Bausk, A.V. Dvurechenskii et al. Application of XAFS spectroscopy to studying the microstructure and electronic structure of quantum dots. J. Surf. Investigation, 1(1), 26.

2009 S.B. Erenburg, S.V. Trubina, N.V. Bausk et al. Microstructure of quantum dots ensembles by EXAFS spectroscopy. J. Physics: Conf. Series, 190, 012131.

2011 S.B. Erenburg, S.V. Trubina, N.V. Bausk et al. An EXAFS Spectroscopy Study of Microstructure of Ensembles of Vertically Coupled Quantum Dots. J. Surf. Investigation. 5 (9), 856.

2013 K. Zhuravlev, T. Malin, S. Trubina, S. Erenburg et al. EXAFS study of GaN/AlN multiple quantum wells grown by ammonia MBE. Phys. Status Solidi C, 10 (3), 311.

S.B. Erenburg, S.V. Trubina, K.S. Zhuravlev et al. Diffusion and deformations in heterosystems with GaN/AlN superlattices, according to data from EXAFS spectroscopy. Bulletin of the RAS. Physics, 77(9), 1147.

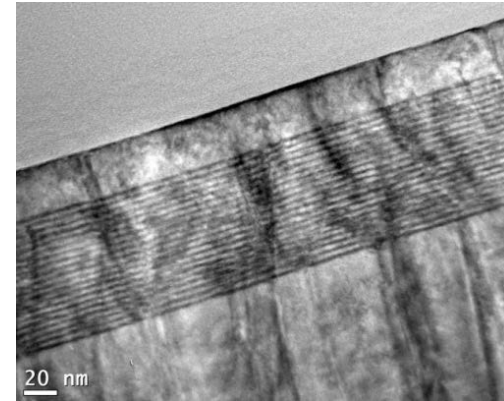
2014 K. Zhuravlev, I. Alexandrov, T. Malin, V. Mansurov, S. Trubina, S. Erenburg et al. EXAFS Study of Intermixing in GaN/AlN Quantum Wells. Proceedings of Intern. Conf. on Manipulation, Manufacturing and Measurement on the Nanoscale (3M-NANO), 27-31 October, Taipei, 100-103.

Ammonia MBE-grown AlN/GaN MQWs

10

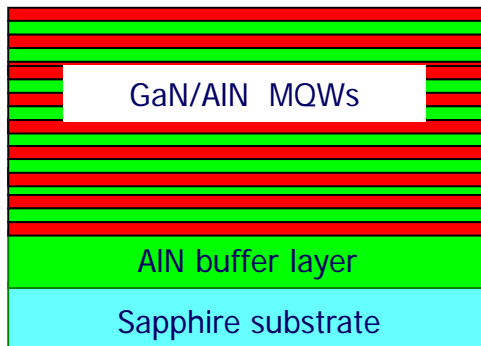


CBE Riber-32

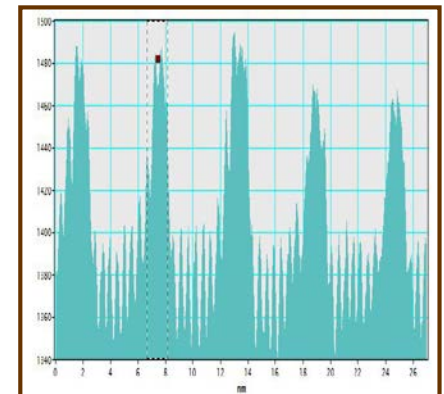
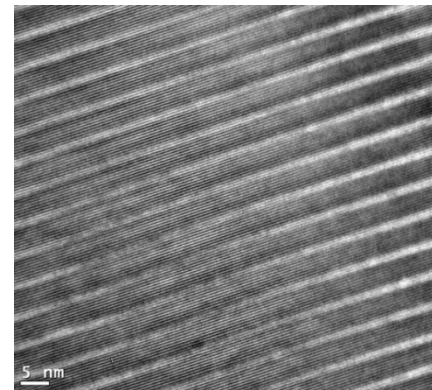


During growth in the process of molecular beam epitaxy of MQW a substrate temperature was kept at 830 °C, an ammonia flux was 200 sccm (standard cubic centimeter per minute).

The high-resolution TEM image of typical the MQWs structure.

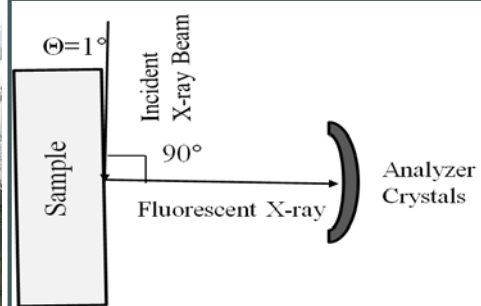
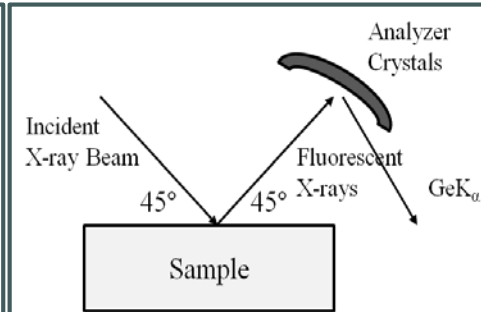
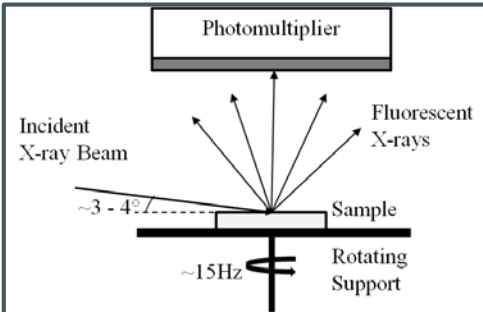
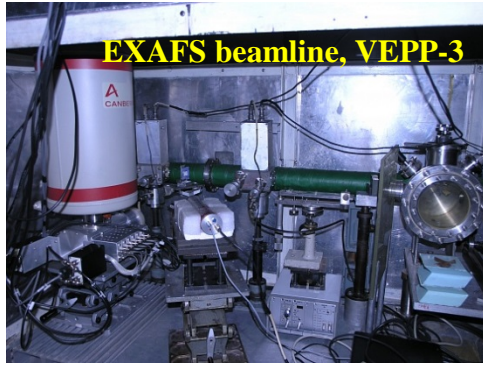


GaN well and AlN barrier thicknesses were varied from 1.0 to 4.0 nm, the number of period was about 20 in thin MQW structures and more than 100 in thick MQW structures.



The HRTEM image and density distribution for the sample 768

Experimental procedures



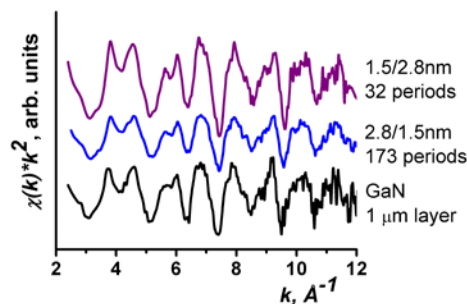
Schemes of spectra measurements: at EXAFS beamline (channel 8) of VEPP-3, BINP SB RAS, Novosibirsk (top left); at the ID26 and ID20 beamlines of ESRF, Grenoble (top right and bottom).

Some part of EXAFS spectra was measured at room temperature at the beamline 8 of VEPP-3, BINP SB RAS. A monoblock slotted monocrystalline Si(111) was used as a crystal-monochromator. The approach with detection of fluorescence X-ray radiation of the sample was used in the integral current mode by a scintillator based on NaI doped by thallium and a modern standard photoelectron multiplier. **The incident angle of X-ray on the sample** was 3-4°. To exclude the influence of the diffraction reflexes of a monochromatic beam of SR from the support, the table with the sample was rotated with the frequency of ~10-15 Hz.

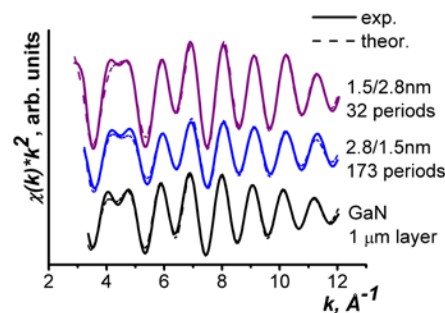
A part of EXAFS spectra were measured at the ID26 and ID20 beamlines of ESRF at temperature 12 K without the sample rotation. The sample, the crystal-analyzers and the detector (cascade photodiode) are located on a vertical Rowland circle. We used at the ID20 beamlines of ESRF two schemes of the relative orientation of the incident monochromatic beam on the sample. In all the schemes the angle between the incident beam on the sample and the direction to the focused crystals was 90°, **the incident angle on the sample** was 1° (ID20) and 45° (ID26).”.

Experimental GaK EXAFS spectra for MQWs

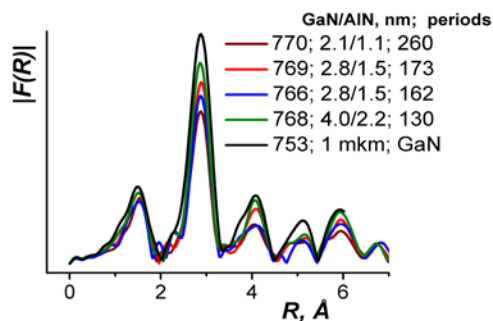
12



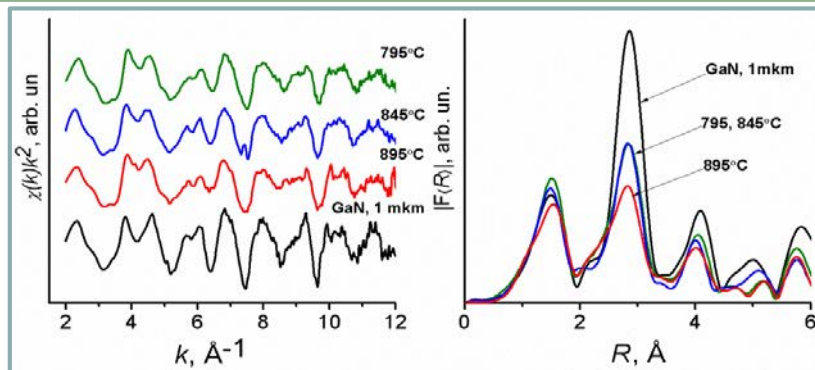
Experimental GaK EXAFS spectra for thin and thick MQW structures with various GaN well, AlN barrier thickness and for GaN film (1 μm).



The Fourier-filtered ($\Delta R=1 - 3.3 \text{\AA}$) experimental and model GaK EXAFS spectra for GaN/AlN MQW structures and GaN film (1 μm).



Fourier transform modules of $\chi(k)k^2$ GaK EXAFS without phase shift for thick MQW structures and for GaN film (1 μm).



Experimental GaK EXAFS spectra and their Fourier transform modules for MQWs structures with various GaN well growth temperatures and for GaN film (1 μm).

EXAFS fit parameters for the MQWs

$2\sigma^2(\text{Ga}) = 2\sigma^2(\text{Al})$, $N_{\text{Al}}=12-N_{\text{Ga}}$, $N_{\text{N}}=4$. GaN и AlN layer thickness estimated from Raman spectra.

“Thick” GaN/AlN MQWs

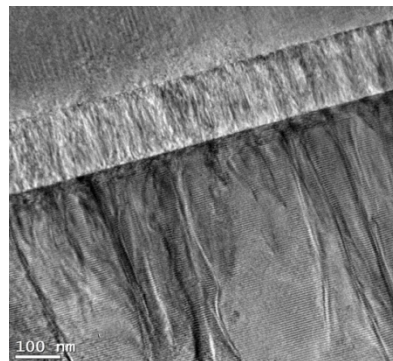
Thickness GaN/AlN, nm	Periods number,	N(Ga)	N(Al)	R(N) Å	R(Ga) Å
GaN bulk; 1mkm		11.9		1.97	3.20
2.8/1.5	130	9.7	2.3	1.95	3.19
4.0/2.2	130	9.9	2.1	1.95	3.18
2.8/1.5	173	9.8	2.2	1.96	3.19
2.1/1.1	260	9.7	2.3	1.96	3.19

“Thin” GaN/AlN MQWs

Thickness GaN/AlN, nm	Periods number	N(Ga)	N(Al)	R(N) Å	R(Ga) Å
1.3/2.5	20	9.3	2.4	1.95	3.16
1.5/2.8	20	9.0	3.0	1.95	3.17
1.5/2.8	22	10.6	1.4	1.95	3.18
1.5/2.8	32	10.6	1.4	1.95	3.17

GaN/AlN MQWs grown by different temperatures

Thickness GaN/AlN, nm	Periods number	T, °C	N(Ga)	N(Al)	R(N) Å	R(Ga) Å
0.9/1.0	30	795	8.9	3.1	1.93	3.15
		845	8.6	3.4	1.93	3.15
		895	8.0	4.0	1.92	3.14

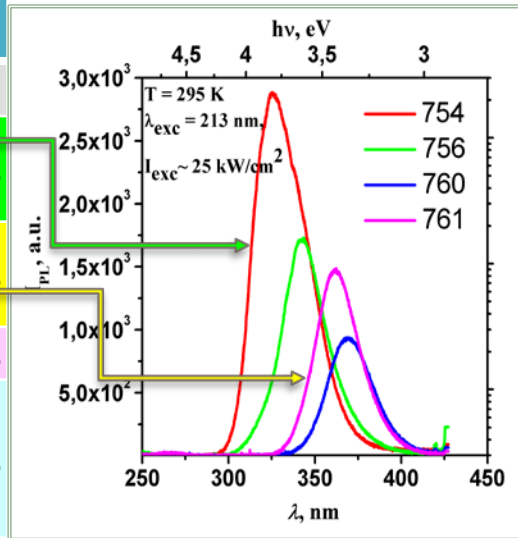


The high-resolution TEM image. Multiple dislocations are observed for the thick structures.

For the thick MQWs the Ga-Ga interatomic distance is at about 0.01 Å lower, than that in the bulk GaN. This result obviously evidences almost full relaxation of the thick GaN layers. For the thin MQWs the Ga-Ga interatomic distance is at about 0.02 -0.04 Å lower, than that in the bulk GaN, that can be due to elastic compression of thin GaN layers in MQWs. Ga-Al intermixing on the heterointerface leads to decrease of the Ga-Ga interatomic distances and Ga-Ga coordination numbers in the MQWs. The intermixing degree in the boundary layers rises from 30% to 40% with increase of the growth temperature from 795 to 895 °C.

Intermixing at GaN/AlN interfaces

N ₀	Thickness GaN/AlN, nm	Number of period	N(Ga)	
753	1mkm		11.9	
754	1.3/2.5	20	9.3	~30%
756	1.5/2.8	20	9.0	
760	1.5/2.8	22	10.6	~10%
761	1.5/2.8	32	10.6	
768	4.0/2.2	130	9.9	~50%
769	2.8/1.5	173	9.8	~40%
770	2.1/1.1	260	9.7	
766	2.8/1.5	130	9.7	



Coordination numbers for the thin samples 760, 761 (yellow) conform to minor ($\leq 10\%$) intermixing in the boundary layers. For thin samples 754, 756 (green) the coordination numbers are slightly lower, consequently, intermixing is higher ($\sim 30\%$). Intermixing is very considerable (up to 50%) for the thick MQWs, that may be due to heating samples at high T for a long time during growth.

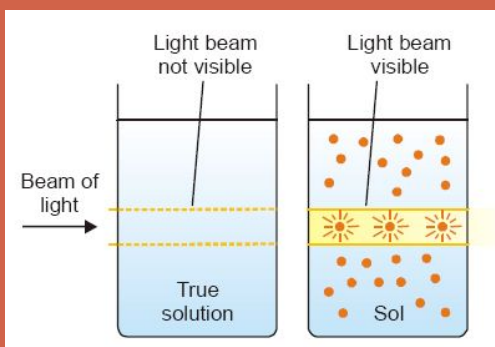
Luminescence maximum shifts to shorter wave-lengths for samples with more pronounced mixing at the interface (754, 756).

Summary MQWs

- It was found that interatomic distances and coordination numbers depend on the total thickness of the MQWs structure. For the thin MQWs the Ga-Ga interatomic distance is at about 0.02 - 0.04 Å lower, than that in the 1 μm thick GaN layer, while for the thick MQWs this difference is 0.01 only. This result obviously evidences almost full relaxation of the thick GaN layers
- The reduced value of R(Ga) may be attributed to compressive strain in the GaN layer of the MQWs.
- The intermixing degree in the boundary layers rises from 30% to 40% with increase of the growth temperature from 795 to 895 °C
- It was shown that intermixing of the heterointerface most pronounced in the thick MQWs. Luminescence maximum shifts to shorter wave-lengths for samples with more pronounced mixing at the interface

Structure of solution

Colloidal solutions contain particles that measure from 1 to 100 nm.



1994 L.N. Mazalov, S.B. Erenburg. X-ray study of electron interactions between sulfide and solvent molecules. *J. Struct. Chem.*, 35(4), 548.

1995 S.B. Erenburg, N.V. Bausk, L.N. Mazalov et al. Structure of palladium chloride complexes with organic sulfides in solutions. *J. Struct. Chem.*, 36(6), 941.

1997 L.N. Mazalov, S.B. Erenburg, N.V. Bausk et al. Studies of the electronic and spatial structure of Cd(II) dialkyldithiocarbamate molecules in nonaqueous media. *J. Struct. Chem.*, 38(4), 601.

1999 S.B. Erenburg, N.V. Bausk, S.M. Zemskova et al. The effect of solvent on the structure of the transition metal complexes in solution. *J. Synch. Rad.*, 6(3), 582.

2000 S.B. Erenburg, N.V. Bausk, L.N. Mazalov et al. EXAFS spectroscopic study on electronic and spatial structure of complex species forming in solutions of coordination compounds. *Inorg. React. Mech.*, 2(1-2), 1.

2001 L.N. Mazalov, N.V. Bausk, S.B. Erenburg et al. X-ray investigation of the structure of metal chelate dithiocarbamate complexes in solution. *J. Struct. Chem.*, 42(5), 784.

2005 S.B. Erenburg, N.V. Bausk, L.N. Mazalov et al. Structure of new heterometallic complexes in hexane on modelling the recovery of ruthenium from radioactive solutions. *Phys. Scripta*, 115, 115.

S.B. Erenburg, N.V. Bausk, L.N. Mazalov et al. Spatial structure of new heterometallic Ru/(Co, Ni, Cu or Zn) complexes in hexane by XAFS spectroscopy. *J. Molec. Liquids*, 118(1-3), 71.

2013 A.I. Petrov, N.N. Golovnev, S.B. Erenburg, et al. Aspectroscopic and ab initio study on Bi(III) complexes formation with 3-mercaptopropanesulfonic acid. *J. Coord. Chem.* 66(23), 4188.

2014 A.I. Petrov, I.D. Dergachev, S.B. Erenburg, et al. Complexation of Bi(III) with 3-mercaptopropionic acid in aqueous solutions: a combined experimental and theoretical study. *RSC Advances*, 4(94), 52384.

2016 S.B. Erenburg, S.V. Trubina, Y.M. Yukhin. Structural characteristics of amorphous K-Bi citrate (De-Nol) and its aqueous solutions from EXAFS spectra. *J. Inorg. Biochem.*

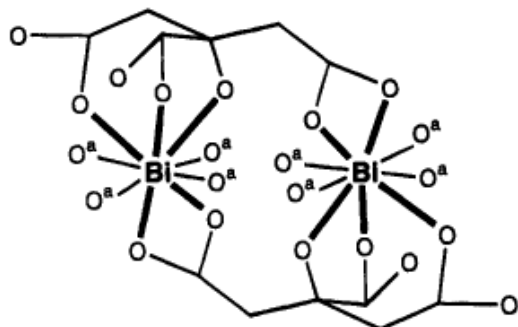
Structural characteristics of amorphous K-Bi citrate (De-Nol) and its aqueous solutions from EXAFS spectra

16

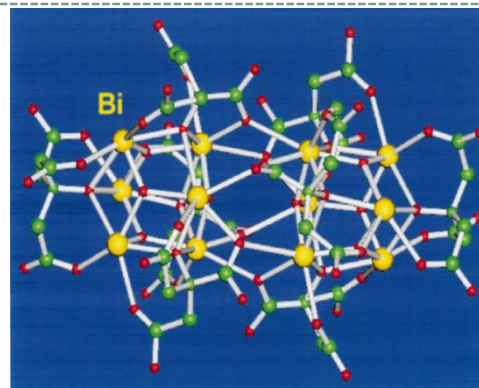
Peptic ulcer is one of the most widespread diseases. In the beginning of the 80's of the last century **it was found that among the causes of peptic ulcer disease one of the main is *Helicobacter pylori* bacterial infection of the mucous coat of stomach.** One of the first antibacterial drugs used for treatment of this infection was De-Nol.

The pharmacologically active part of the drug is colloidal bismuth subcitrate (CBS) consisting of a complex of basic bismuth citrate ($\text{cit}=\text{C}_6\text{H}_4\text{O}_7^{4-}$) and potassium and ammonium citrates dried from the ammonia colloidal solution. The drug is different from other bismuth salts in that it can dissolve in gastric mucus which allows it to penetrate to *Helicobacter pylori* under its layer. **The solubility of colloidal bismuth subcitrate is 100 times higher than that of other bismuth-containing drugs.**

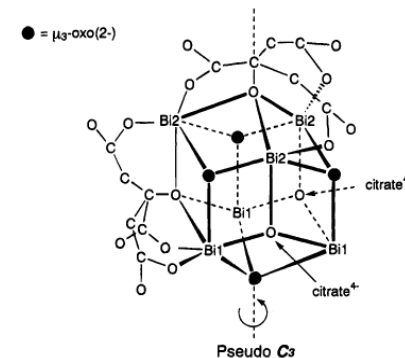




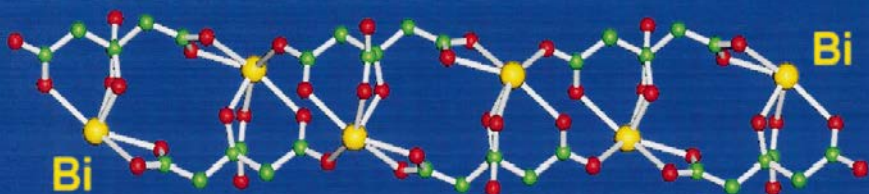
Common dinuclear subunit (cit^{4-})BiBi(cit^{4-}) on bismuth citrate compounds.



Structure of the $\text{Bi}_{12}\text{O}_{22}$ cluster core.



$[\text{Bi}_6\text{O}_4(\text{cit}^{4-})_4]^{6-}$



Polymeric anionic chain of $[\{\text{Bi}(\text{cit})_2\text{Bi}\}_n]^{2n-}$

I Although **biologically active complexes based on Bi citrate have long been widely used in medicine**, studies of the structure of the complexes have been started relatively recently. We are aware of at least nine different crystalline forms of bismuth citrate, which were characterized by X-ray diffraction. **In these compounds, the main structural element is a stable dimeric (cit^{4-})BiBi(cit^{4-}) moiety.**

II The investigation of the structure of the complex in aqueous solutions appears to be especially important because the drug acts just in solution and the optimization of its medicinal properties through the variation of structural characteristics of the complex in solution can turn out to be very significant. It should be noted here that the pharmaceutical effect of the drug depends on its state (a solid pill or a solution) and also on the concentration of the active drug component in solution. **Special attention should also be paid to the structural features of a crystal composed of 12-nuclear $\text{Bi}_{12}\text{O}_{22}$ clusters and its behavior in solutions.**

EXAFS experiment

18

Measurements were carried out on a synchrotron radiation channel of the VEPP-3 storage ring at the Budker Institute of Nuclear Physics, SB RAS.

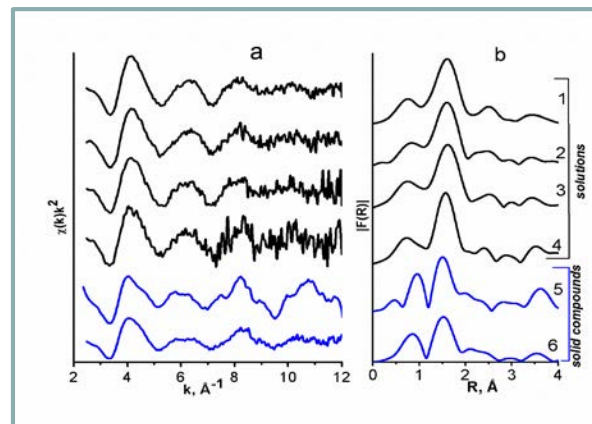
We have studied the following systems:

Aqueous solutions of colloidal bismuth subcitrate:

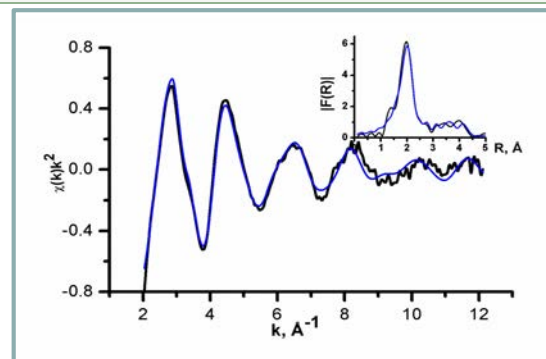
- ❖ A concentrated solution with a bismuth concentration of ~ 370 g/L;
- ❖ A threefold diluted concentrated solution;
- ❖ A fivefold diluted concentrated solution;
- ❖ A tenfold diluted concentrated solution;

Solid complexes of dried colloidal bismuth subcitrate:

- ❖ A sample of dried colloidal subcitrate (synthesized in the Inst. of Sol. State Chem.)
- ❖ Medicine tablet (Yamanouchi Europe).



Experimental $k^2\chi(k)$ BiL_{III} EXAFS spectra of samples (a) and their Fourier transform magnitudes $|FT|$.



Experimental $k^2\chi(k)$ Bi L_{III} (black line), model (blue line) EXAFS spectra of saturate water solution, and their Fourier transform magnitudes $|FT|$ (inside figure)

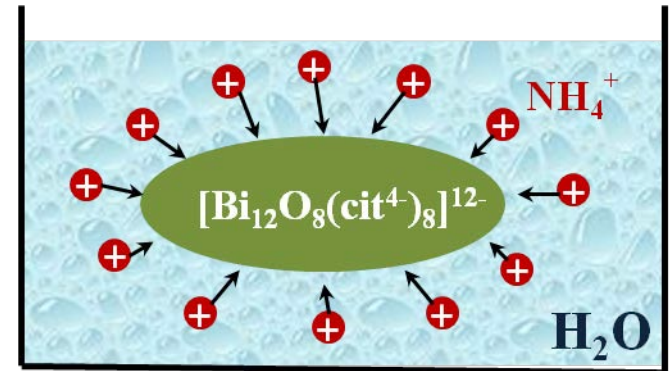
Structural data for crystal containing Bi ₁₂ O ₂₂ clusters			EXAFS models										
			Water Solutions								Amorphous Solid Compounds		
	Average Distances R, Å	Coord. Number N	Saturated		1:3		1:5		1:10			R, Å N	
			R, Å	N	R, Å	N	R, Å	N	R, Å	N		R, Å	N
Bi-O	2.187	2	2.14	1.8	2.15	2	2.15	1.9	2.15	2	Bi-O	2.08	1.0
Bi-O	2.28	2	2.33	1.7	2.35	1.9	2.34	1.6	2.36	1.5	Bi-O	2.34	0.9
Bi-O	2.50	1	2.56	1.2	2.59	1.2	2.59	1.2	2.63	1.3	Bi-O	2.57	2.5
Bi-O	2.82	2	2.89	2.1	2.93	2.1	2.93	2.2	2.99	2.8	Bi-O	2.85	2.8
											Bi-O	3.06	1.0
Bi-Bi	3.73	4	3.72	4.0	3.71	4.0	3.70	4.0	3.66	4.0	Bi-Bi	4.0	2.1

In the EXAFS simulation the starting model was based on the crystallographic structural data for the (NH₄)₁₂[Bi₁₂O₈(cit)₈](H₂O)₁₀ complex. **As seen from Table, the structure of the Bi environment for the complexes in droplet particle in the colloidal solution is close to the structure of the nearest spheres of the Bi environment in the 12-nuclear Bi clusters.** When the solution is diluted, the cluster structure is somewhat modified, it remaining very similar to the structure of the Bi₁₂O₂₂ cluster. It is worth noting that according to the crystallographic data, the (NH₄)₁₂[Bi₁₂O₈(cit⁴⁻)₈](H₂O)₁₀ **cluster has a size of 8684 Å³. This size corresponds to a particle diameter of ~20 Å and is well consistent with the preliminary data obtained by small-angle X-ray scattering for cluster sizes in the concentrated solutions (~20 Å).** Some increase in the sizes in diluted solutions (from ~20 Å to ~26 Å) was found here (in the small-angle X-ray scattering experiment) agrees with our data on an increase in coordination number with respect to oxygen when **hydroxyl groups (Bi-O~3.0 Å) are incorporated into the structure of the Bi₁₂O₂₂ cluster.** **The structure of the amorphous solid complexes (standard sample of the drug and synthesized in the laboratory) apparently is multiphase, but, as a whole, is similar to the structure of the binuclear solid complexes with a noticeable polymerization (N_{Bi-Bi} ~ 2).**

Summary of colloidal bismuth subcitrate (De-Nol)

20

➤ The structure of the Bi environment in the CBS complexes in solution is close to the structure of the nearest spheres of the Bi environment in the crystalline $(\text{NH}_4)_{12}[\text{Bi}_{12}\text{O}_8(\text{cit}^{4-})_8](\text{H}_2\text{O})_{10}$ compound composed of 12-nuclear Bi clusters.



➤ When the solution is diluted, the cluster structure is somewhat modified, it also remaining similar to the structure of the $\text{Bi}_{12}\text{O}_{22}$ cluster. The appearance of an additional oxygen atom at a large distance from the bismuth atom ($\sim 3.0 \text{ \AA}$) when the solution is tenfold diluted, is due to the presence of the hydroxyl group from the aqueous solution.

➤ The structure of the amorphous solid complex is multiphase, but, as a whole, similar to the structure of the solid binuclear complex and very different from the structure of the 12-nuclear cluster and CBS complexes in solution.

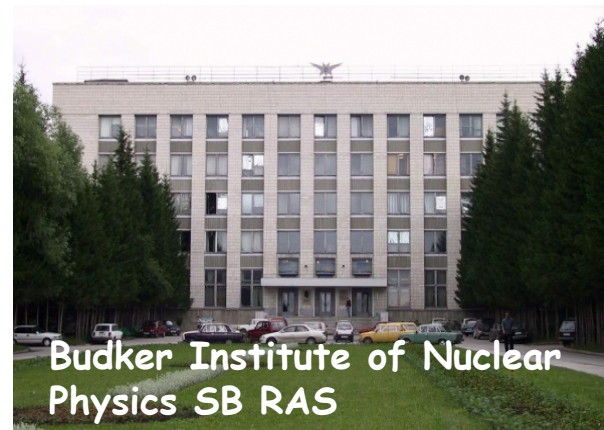
➤ Specific structural features of complexes in solution can be important for the pharmaceutical effect of CBS complexes.



Nikolaev Institute of Inorganic
Chemistry SB RAS



Rzhanov Institute of
Semiconductor Physics SB RAS



Budker Institute of Nuclear
Physics SB RAS

Thank you for attention!



Boreskov Institute of
Catalysis SB RAS



Institute of Solid State
Chemistry and Mechanochemistry
SB RAS



ESRF, Grenoble, France